Soft Matter

PAPER

View Article Online
View Journal | View Issue

Cite this: *Soft Matter*, 2018, **14**, 5106

Quenching of fully symmetric mixtures of oppositely charged microgels: the role of soft stiffness†

Thiago Colla, *[ab] Ronald Blaak [b] and Christos N. Likos [b]

Received 4th March 2018,
Accepted 14th May 2018

DOI: 10.1039/c8sm00441b

rsc.li/soft-matter-journal

Using molecular dynamics simulations, we investigate the self-assembly of a coarse-grained binary system of oppositely charged microgels, symmetric in size and concentration. The microgel pair interactions are described by an effective pair potential which implicitly accounts for the averaged ionic contributions, in addition to a short-range elastic repulsion that accounts for the overlapping of the polymer chains, the latter being described by the Hertzian interaction. Particular emphasis is placed on the role played by the strength of the soft repulsive interaction on the resulting particle aggregation. It is found that the possibility of particle inter-penetration in oppositely charged soft particles results in a much wider variety of cluster morphologies in comparison with their hard-spheres counterparts. Specifically, the softness of the steric interactions enhances the competition between repulsive and attractive electrostatic interactions, leading to the formation of aggregates that are comprised of strongly bounded charged particles displaying a low degree of charge ordering.

1 Introduction

One of the ultimate goals of material science is to design particle systems with well controllable macroscopic properties, which can be easily adapted to conditions suitable for practical applications.[1,2] In this sense, soft-matter systems in general can be viewed as excellent building blocks for the development of complex materials with tunable properties.[2–7] With typical size scales ranging from a few Ångströms to micrometers, the components of these systems can be properly combined to provide a rich variety of assembly behavior, whose dynamical and morphological properties can be experimentally controlled.[2,8–12] In some situations, the inherent length scale of the components involved offers the unique opportunity to track down in real time the dynamics of assembling structures through experimental techniques such as video-microscopy.[13–15] The theoretical prediction of such structures, however, requires not only the knowledge on how the various components interact with each other,[4,16] but also on what are the physical mechanisms behind such interactions that drive the system to particle aggregation.[1,17] This is in general a difficult task, since very simple interactions in multicomponent systems can already give rise to some very complex assembling structures.[18,19] In the case of monodisperse systems, one crucial ingredient that leads to complex structural and thermodynamic behavior is the combination of short-range repulsion and long-range attractive interactions.[20–24] Short-range purely attractive potentials between nanoparticles – usually resulting from the van der Waals (vdW) forces or depletion interactions[23] – are known to result in irreversible particle aggregation, in which case the clustering process is controlled by particle diffusion.[18] A simple model system able to qualitatively capture the main features of the underlying irreversible particle assembling is the so-called sticky sphere model, whereby the particles are represented by hard spheres that stick together as soon as they come in contact to each other.[25–27] Even this simple diffusion-limited aggregation scenario can lead to a complex variety of cluster structures in monodisperse systems.

The aforementioned complexity increases considerably when the system is comprised by different interacting components, which is the case for the vast majority of soft-matter systems. In many situations, the various components differ by orders of magnitudes in their typical sizes.[4] In such a case, the system is usually represented as a monodisperse suspension, whose particles interact *via* an effective potential that implicitly contains the averaged effects from the smaller components.[16,28,29] This feature can be conveniently used to render nanoparticles the desirable effective interactions by tuning the properties of the small scale components – such as their concentration, size,

[a] *Instituto de Física, Universidade Federal de Ouro Preto, CEP 35400-000, Ouro Preto, MG, Brazil*
[b] *Faculty of Physics, University of Vienna, Boltzmanngasse 5, 1090 Vienna, Austria. E-mail: thiago.escobar.colla@univie.ac.at*

† Electronic supplementary information (ESI) available. See DOI: 10.1039/c8sm00441b

charge, magnetization or dipolar moment – once the underlying averaged effects are known. In a similar fashion, the assembly of nanoparticles can be adjusted in order to engineer macroscopic structures with controllable architectures.[30] A usual strategy is then to investigate the coarse-grained interactions between the nanoparticles, from which the phase behavior underlying the structural formations can be inferred.[16,31,32] A reversed designing approach, in which the effective interactions that might give rise to specific assembling structures is sought for, has quite recently been the subject of intensive investigation.[33–36] Although such approaches can provide valuable insights on the physical mechanisms responsible for particle aggregation, it is not always clear how feasible such effective interactions are from an experimental perspective. In this sense, the study of coarse-grained interactions in soft-matter systems represents a powerful tool not only for the understanding of the various complex assembling mechanisms in biological and chemical systems, but also for providing reliable guidelines towards the design of complex materials.

In the case of systems composed of a mixture of macroscopic particles that bear similar length scales, the strong competing interactions usually result in rich phase diagrams characterized by complex assembling structures. Such strong interaction might in many cases lead to dynamically arrested structures, generally characterized by amorphous cluster formations.[37] This is the case, for instance, for gelation or glass formation in charged colloidal systems, whereby the system is known to become trapped in long-lived assembling structures on its pathway to a binodal decomposition.[37–39] In such cases, computer simulations are particularly useful to shed light on the underlying cluster formation, along with its dynamical properties.[40] When the nanoparticles bear charges of opposite sign, the electrostatic attraction at particle contact might strongly exceed the entropic contributions, leading to irreversible particle aggregation.[41–46] Such nanoparticles are usually modeled as hard-spheres with Yukawa-like interactions beyond particle contact,[47] the screening length of which can be conveniently controlled by addition of 1 : 1 electrolyte. In the limit of very short screening lengths, this model system can be well described by a two component version of the aforementioned sticky sphere model. The possibility of tuning the range of the competitive interactions by changing the screening lengths, as well as their strengths by adjusting the relative charge asymmetry, results in the formation of arrested states characterized by complex assembling morphologies.[43]

A similar model system can be applied for the case of charged soft nanoparticles, such as ionic microgels. One key difference is that microgel particles are composed of a shell of loosely cross-linked polymer chains, which are permeable to both ionic species and solvent molecules.[48] This property renders microgel particles very versatile with respect to changes in their surrounding conditions, making them particularly promising in a number of applications involving the development of responsive materials[49,50] such as chemical separators[51,52] and reactors.[53,54] One example is the volume transition in these particles, which is dictated by the chemical equilibrium with the external solvent,[55] and depends crucially on quantities such as the solvent quality,[56–58] the temperature,[55,59] the amount of added electrolyte[60,61] and the cross-linking morphology.[62,63] This size-dependence on the medium properties and the ability of particle exchange can be conveniently applied in the designing of drug-delivery systems.[64,65] Other than in hard colloids, the short-range repulsion in microgels are described by a soft potential when particles overlap, resulting from elastic deformations of their polymer chains under compression. Due to this soft nature, microgels are allowed to partially penetrate each other, and can therefore reach very high packing fractions.[66] When combined with an attractive tail, this interaction can result in a potential well that can even be found within the overlapping range. It is hence clear that this property can have a non trivial effect on particle aggregation. Quite recently, a series of experimental investigations has been performed in which attractive dipolar interactions in ionic microgels are induced by an external AC electric field, revealing a strong degree of inter-particle penetration along the field direction.[67–69] With respect to the self-assembly structures driven by competitive interactions, it is expected that such soft particles will be allowed to pack in much more compact aggregates in comparison to equally sized hard particles.[70,71]

A system of ionic microgels with opposite bare charges has been recently devised experimentally by properly adjusting the degree of ionic polymerization of their polymer backbones through changes in the solvent pH.[72] This mechanism allows not only to synthesize microgels bearing opposite charges, but also to dynamically change the particle charge asymmetry and to track down its effects on the underlying bulk particle aggregation. Along the same lines, a system of oppositely charged microgels has been used to experimentally investigate particle assembly at dielectric interfaces.[73] Even though the nano-scaled assembling properties of hard colloidal systems with different charge asymmetries have been already investigated using both computer simulations[42,43,46] and theory,[74,75] a similar study for the cluster morphology in a system of oppositely charged ionic microgels is still lacking. In particular, the effects from the softness of the elastic short-range repulsion on the particle aggregation in these systems have not been investigated in detail.

The aim of this work is to address this question, giving emphasis on the dependence of the assembling structural properties on the strength of the repulsive elastic interactions. To this end, a recently developed coarse-graining model potential for ionic microgels with different charges will be applied.[76] This ionic averaged effective interaction will be combined with a Hertzian potential that describes the short-range elastic repulsion upon particle overlapping.[77] By tuning the strength of the Hertzian potential, both the depth and position of the potential well for oppositely charged microgels can be controlled, and therefore the degree of particle penetration. Using the liquid state integral equations approach, it was shown that the extend to which particles overlap has a major effect on the system structure.[76] In order to assess its effects on the cluster formation in the case of higher electrostatic couplings – where

the validity of the integral equation approach breaks down – we will here perform Molecular Dynamics (MD) simulations for the system of oppositely charged microgels.

The work is organized as follows. In Section 2, a short description of the effective interactions between the binary microgels is given. The model system to be used in the analysis of particle self-assembly is described in Section 3. Both qualitative and quantitative results are shown and discussed shortly afterwards in Sections 4–6. Finally, concluding remarks are given in Section 6. In the ESI† we provide videos from our simulations, showing the self-assembly processes of microgel mixtures for various combinations of values of the coupling parameters (charge, screening length and elasticity).

2 Coarse-grained interactions

We consider a two-component system of ionic microgels in solution, bearing charges of the same magnitude but with opposite sign. The binary system is completely symmetric in the sense that all particles have the same relative concentrations and are equally sized. Apart from the macroscopic microgels, the solution also contains dissociated monovalent counterions released from their charged backbones, in addition to added 1 : 1 electrolyte. The solvent is treated as a continuous aqueous environment of permittivity $\epsilon = 80$. We consider here solutions at room temperature, for which the Bjerrum length $\lambda_B = \beta q^2/\epsilon$ (where q represents the charge of a proton and $\beta = 1/k_BT$ the inverse temperature) assumes the value $\lambda_B = 7.2$ Å. We work at a linear, coarse-grained level description,[76,78,79] in which the ionic contributions are explicitly averaged out, rendering the electrostatic interactions outside particle overlap screened. The microgels are modeled as spherical objects of radius R_i with a charge Z_i uniformly distributed over their volume core. This picture has been extensively used to describe loosely cross linked microgels at their swollen sate, where the inhomogeneous character of the monomer distribution can be disregarded. Under these circumstances, the ionic-averaged electrostatic pair potential $u_{ij}^{\mathrm{elec}}(r)$ between two microgels of radii R_i and R_j (assuming, without loss of generality, $R_i > R_j$) and charges Z_i and Z_j can be separated into three regions:‡

$$\beta u_{ij}^{\mathrm{elec}}(r) = \frac{9Z_iZ_j\lambda_B}{2\kappa^6R_i^3R_j^3}\left[\frac{2}{3}\kappa^4R_j^3 - 2F(\kappa R_j)\mathrm{e}^{-\kappa R_i}(\kappa R_i+1)\frac{\sinh(\kappa r)}{r}\right], \quad (1)$$

valid at the overlapping region where $0 \le r \le R_i - R_j$, where

$$F(x) \equiv x\cosh(x) - \sinh(x). \quad (2)$$

The parameter κ represents the inverse Debye screening length provided by the ionic clouds surrounding the microgel particles.

‡ There is a typo in eqn (54) of the original paper, ref. 76. In the second term within the square brackets of the right-hand side of this equation, the factor 3 should be replaced by 2, and the factor $\mathrm{e}^{\kappa R_\alpha}$ should be $\mathrm{e}^{-\kappa R_\alpha}$ (note that in this manuscript the notation changes $R_\alpha \to R_i$ and $R_\beta \to R_j$ with respect to the notation in ref. 76 have been made). The expression provided here, eqn (1), is the correct one.

For the remaining overlapping region $R_i - R_j < r < R_i + R_j$, the pair potential reads:

$$\begin{aligned}\beta u_{ij}^{\mathrm{elec}}(r) = \frac{9Z_iZ_j\lambda_B}{2\kappa^6R_i^3R_j^3r}\Big[&\gamma_{ij}(r) + F(\kappa R_i)(\kappa R_j+1)\mathrm{e}^{-\kappa(r+R_j)} \\ &- \mathrm{e}^{-\kappa R_i}(\kappa R_i+1)\big(\kappa R_j\sinh[\kappa(r-R_j)] \\ &+ \cosh[\kappa(r-R_j)]\big)\Big].\end{aligned} \quad (3)$$

The function $\gamma_{ij}(r)$ introduced above is defined as:

$$\begin{aligned}\gamma_{ij}(r) = \frac{\kappa^4}{2}\Bigg[&\frac{1}{2}(R_i^2-r^2)\left(R_j^2-(r-R_i)^2\right) + \frac{2r}{3}\left(R_j^3-(r-R_i)^3\right) \\ &- \frac{R_j^4}{4} + \frac{(R_i-r)^4}{4}\Bigg] + \frac{\kappa^2}{2}(r^2-R_i^2-R_j^2) + 1.\end{aligned} \quad (4)$$

At the region outside the microgel cores, $r \ge R_i + R_j$, the electrostatic pair potential assumes a familiar Yukawa-like form:

$$\beta u_{ij}^{\mathrm{elec}}(r) = \frac{9Z_iZ_j\lambda_B}{\kappa^6R_i^3R_j^3}F(\kappa R_i)F(\kappa R_j)\frac{\mathrm{e}^{-\kappa r}}{r}. \quad (5)$$

For the case of equally sized microgels considered here, only the last two above equations with $R_i = R_j \equiv R$ are necessary to fully specify the electrostatic interactions. Contrary to the case of hard colloids, which experience an infinity repulsive force at close contact, microgels undergo a soft elastic-like repulsion resulting from the mutual deformation of their polymer chains under compression, in addition to the electrostatic interactions described by eqn (1) and (3). The soft repulsion is assumed to be well-described by the Hertzian potential:[77]

$$\beta u_H(r) = \begin{cases}\varepsilon\left(1-\frac{r}{\sigma}\right)^{5/2} & r \le \sigma, \\ 0 & r > 0,\end{cases} \quad (6)$$

where $\sigma = 2R$ is the particle diameter and ε is a dimensionless parameter which corresponds to the strength of the soft repulsion. This quantity is related to the particle size, system temperature and material elastic properties through

$$\varepsilon = \frac{2\beta Y\sigma^3}{15(1-\nu^2)}, \quad (7)$$

where ν is the Poisson's ratio and $Y = 3K(1-2\nu)$, with K being the characteristic bulk modulus of the macroscopic, cross-linked elastic solid. Notice that this parameter will assume different values for the interaction between particles bearing different sizes. In the present case of charge symmetric components, we will assume that all microgels have the same elastic properties, and therefore the parameter ε will assume the same values for all microgels.

At this point, it is important to emphasize the main physical assumptions underlying the adopted soft Hertzian repulsion. In this simplified approach, it is assumed that particles can change neither internal morphology nor shape upon strong overlapping. These assumptions will clearly break down in cases of microgels made up of close-packed polymer chains with a high degree of internal cross-linking. On the other hand, they should be quite reasonable when dealing with microgels in

their swollen state. In the latter case, the microgels feature a dense core and a very dilute layer of loosely cross-linked polymer chains. The overlapping layers of approaching microgels will undergo an elastic soft repulsion which can be quite well described by the Hertzian approach, without any significant changes in their internal charge conformations – even at strong overlapping. We therefore expect that the model system and results to be outlined in what follows will be well suited to describe microgels in their swollen state, but should be questionable in situations of highly compact, core-like microgels.

The total, effective microgel pair potential $\beta u_{ij}(r) = \beta u_{ij}^{\mathrm{elec}}(r) + \beta u_{\mathrm{H}}(r)$ is given by the combination of the electrostatic and soft interactions described by eqn (1), (3) and (6). The resulting interaction between dissimilarly charged microgels features the competition between a long-range electrostatic attraction and a short-range elastic/steric repulsion. The relative strength of these competing interactions can be tuned by properly changing system parameters such as the particle charge Z and the screening length κ^{-1} – which controls respectively the strength and range of the electrostatic interactions – as well as the strength of Hertzian repulsion ε. When the latter is large enough such as to strongly overcome the electrostatic attraction at contact, particle interpenetration is suppressed and the limit of charged hard colloids is recovered. In the opposite limit where ε is not too high, particles are allowed to penetrate one another in order to minimize the overall electrostatic energy. It is the interplay between these different mechanisms – electrostatic bounding of oppositely charged particles and soft repulsion at close contact – that will dictate the way particles will locally aggregate into either compact or open-like structures.

3 Model system

We now briefly outline the model system under investigation. We shall consider two distinct samples of binary particles, one bearing a moderate charge of $Z = 300$ and the other one with a higher charge $Z = 500$. In all cases, the particle diameters are $\sigma = 1.4$ μm and the concentrations of each charged component is fixed at $\rho_{\pm}\sigma^3 = 0.075$, corresponding to individual packing fractions of $\phi_{\pm} \approx 0.04$. In both cases we consider two different screening parameters $\kappa\sigma = 1$ and $\kappa\sigma = 3$, corresponding to moderate and small Debye screening lengths $\xi = \sigma$ and $\xi = \sigma/3$, respectively. Fig. 1 shows how the effective interactions for both dissimilarly $\beta u_{+-}(r)$ (left-hand panels) and similarly $\beta u_{++}(r)$ (right-hand panels) charged particles behave for the considered system parameters and at different strengths of Hertzian repulsion, ε. The attractive effective potentials feature a potential well which describes the short-range competition between electrostatic attraction and soft repulsion. Notice that the potential depth lies in all cases deep inside the particle overlapping range ($r < \sigma$) provided the particle stiffness becomes sufficiently small ($\varepsilon \leq 100$). The potential minimum is quickly shifted to larger distances (near to particle close-contact $r \approx \sigma$) as the particle stiffness ε increases and, at the same time, becomes shallower and sharper in shape. The presence of such potential wells clearly indicates that oppositely charged particles will associate at distances that are dictated by the degree of particle softness. The deeper well at small ε means that particles will be strongly connected in this case. Also, the fact that the potential wells are broader in this limit suggests that particles will be more susceptible to thermal fluctuations around their relative equilibrium positions. On the other hand, the presence of shallow and sharp potential wells for stiff particles is an indication that particles will be more localized – though less connected – in these cases. All such effects that arise from the competition between soft and electrostatic interactions are enhanced as the electrostatic coupling grow higher (*i.e.*, high charges and small inverse screening lengths). On the other hand, the repulsive effective interactions become increasingly stronger as the particle stiffness increases (right panels). These effects are more pronounced

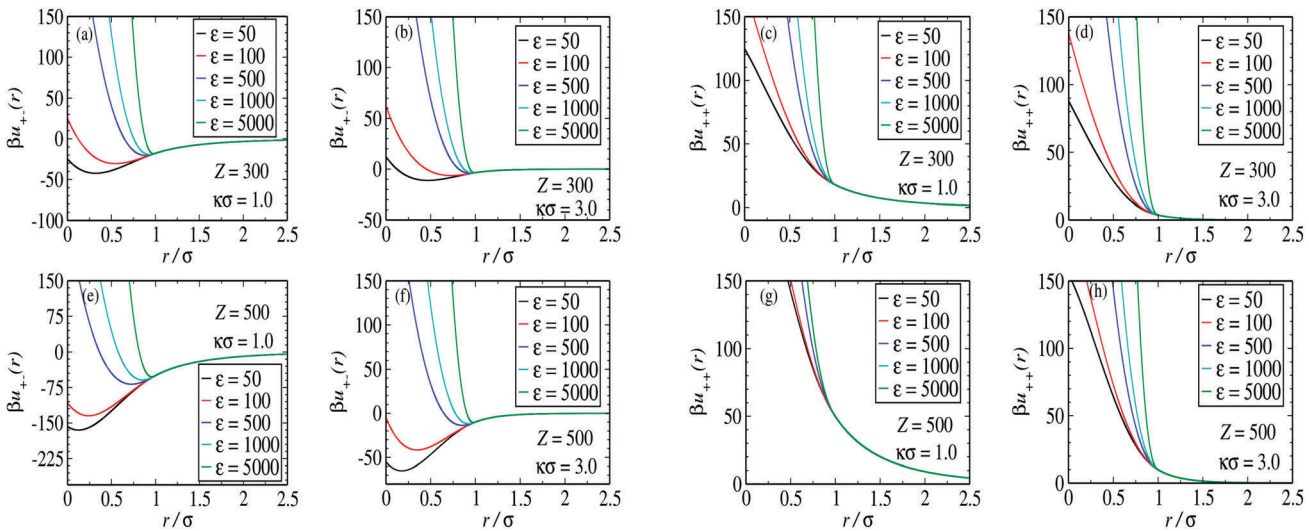

Fig. 1 Effective pair potential between oppositely (left panels) and equally (right panels) charged soft microgels at different Hertzian strengths ε. The microgel charges are $Z = 300$ (upper panels) and $Z = 500$ (lower panels), while the inverse Debye screening lengths are given by $\kappa\sigma = 1.0$ and $\kappa\sigma = 3.0$. In all cases the binary microgels are equally sized, with particle radii $R = 0.7$ μm.

at weak electrostatic couplings, where electrostatic and elastic repulsions have similar order of magnitudes. Interesting enough, the contact energy between equally charged pairs decreases significantly when the inverse screening length increases from $\kappa\sigma = 1$ to $\kappa\sigma = 3$. This reduction in the energetic penalty for bringing two particles of the same charge close together will enhance the competition between electrostatic repulsive and attractive interactions, favoring thus the formation of compact aggregates. We now turn to the analysis of particle aggregation for the system of microgels interacting through the potentials depicted in Fig. 1.

4 Results and discussion

In order to investigate the particle self-assembly of the model system described above, we have performed *NVT*-molecular dynamic (MD) simulations. A total of $N_+ = 500$ positive and $N_- = 500$ negatively charged particles are randomly put together in a cubic simulation box of sides $L = (\rho/N)^{-1/3} = 33.2$ μm. Periodic boundary conditions have been applied across the simulation walls, and a cut-off distance of $r_c = 4\sigma$ has been taken for the truncation of particle interactions. From the initial random distributions, the equations of motion were integrated using the usual Verlet algorithm, and the system was quenched to the desired temperature using a Andersen thermostat. A time step of $\delta\tau = 10^{-3}\tau_0$ has been used, where $\tau_0 = \sqrt{m\beta\sigma^2}$ is the typical system time scale (m is the microgel mass). A total of $N_s = 4 \times 10^6$ time steps – long enough to ensure equilibration of static properties such as pair distributions and overall energy – have been considered for all the samples. Relaxation to the target temperature is in all cases achieved after a simulation time of $\tau \approx 30\tau_0$.

4.1 Qualitative analysis

We start the investigation of particle self-assembly by performing a qualitative analysis that will help us understanding the effects of changing both particle softness and ionic strength on the underlying cluster morphology. To this end, we show in Fig. 2 and 3 simulation snapshots of typical static configurations for samples corresponding to $Z = 300$ (Fig. 2) and $Z = 500$ (Fig. 3). Top panels are results for moderate screened interactions ($\kappa\sigma = 1$), whereas bottom panels stem from strong screening systems ($\kappa\sigma = 3$). From left to right, the degree of particle stiffness (or equivalently ε) increases. A rich morphology of particle aggregates can be observed. For $Z = 300$ and $\kappa\sigma = 1$ (upper panels of Fig. 2), particles are arranged in crystal-like local structures of alternating negative (red balls) and positive (gray balls) particles. As ε increases, the aggregates begin to "open up", becoming larger in size. This is a clear effect of the larger averaged inter-particle distances as particles become harder. A quite different scenario is observed when the interactions become more screened (bottom panels of Fig. 2). In this case, the microgels aggregate into rather amorphous, compact clusters, which start to break up as particle stiffness increases. A behavior that is reminiscent of a liquid droplet approaching the critical point. Again, this detachment of particles from the aggregates results from the induced increase in inter-particle separations for larger ε (notice that even some isolated monopoles can be found in this case). For such strong elastic repulsions, the interactions are not strong enough to sustain the formation of stable clusters, and the dynamics is dominated by thermal motion (see ESI† for selected movies that display the dynamic evolutions).

The situation changes dramatically in the case of strongly charged microgels ($Z = 500$, see Fig. 3). Here the particles do not aggregate in compact clusters. Instead, they assemble into open percolating structures characteristic for gel-like states. For weak soft interactions and screenings, particles are combined to form large inter-connected networks. These "worm-like" percolating structures are a result of the merging of long chains at the early beginning of system quenching (see ESI†). As the particle becomes harder, these structures start to fold into large aggregates with

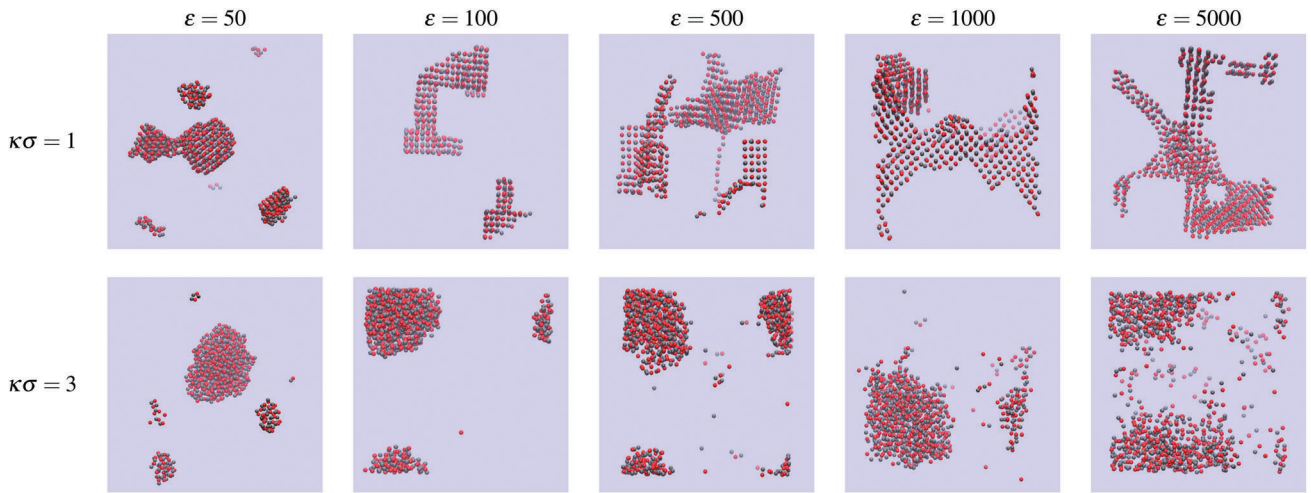

Fig. 2 Simulation snapshots for the binary symmetric system of oppositely charged microgels with charge $Z = 300$ and inverse Debye screening lengths $\kappa\sigma = 1$ (upper panels) and $\kappa\sigma = 3$ (lower panels). Red balls represent negatively charged particles, while gray balls are positively charged microgels. From left to right, the Hertzian strength parameters are $\varepsilon = 50$, 100, 500 and 5000. All snapshots have been taken at the latest simulation time-step, $\tau = 4 \times 10^3\tau_0$.

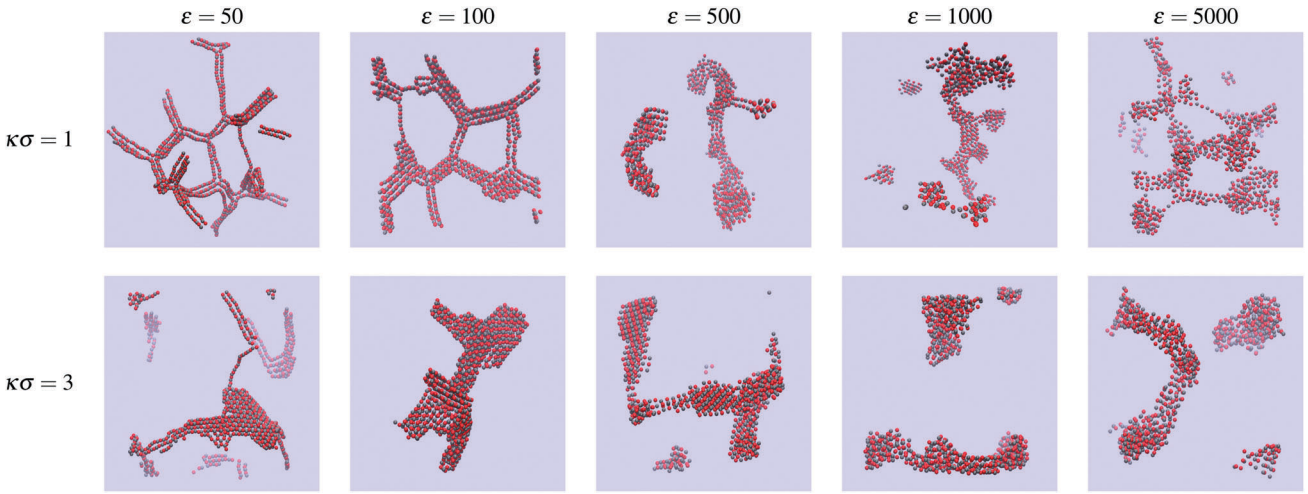

Fig. 3 Same as in Fig. 2, but with a larger microgel charge of Z = 500.

more compact local structures. In this parameter region, the induced increase in particle distances makes the formation of long chain-like structures unstable, and the formation of compact structures becomes energetically favorable. As we shall see later on, this behavior results from a decrease in the competition between attractive and repulsive electrostatic interactions.

Having presented the qualitative effects of changing electrostatic couplings and particle stiffness on the particle aggregation, we now proceed to perform a detailed quantitative investigation of these effects.

5 Dynamics

We are now going to explore how the particle stiffness – as modeled by different strengths of the Hertzian elastic repulsion – will influence the aggregation process and the underlying cluster structure in the model system described above. We first notice that, in contrast to purely hard nanoparticles, the ability of oppositely charged soft particles to mutually interpenetrate gives rise to an aggregation process which is mostly dynamically driven: as soon as a pair of oppositely charged particles encounter each other, they will most likely stick together in an attempt to minimize their mutual electrostatic energy. This is because the proposed model system assumes the absence of any volume transitions in the kinetic of cluster aggregation. If, on the other hand, particles are allowed to deswell in response to the strong elastic repulsions under compression, the timescales of volume transitions may play an important role in the overall dynamics of particle self-assembly. Taking into account this swelling behavior at a dynamical level is however a quite challenging task, which goes way beyond the scope of the present approach.

The binding process is in the present case much more robust against thermal fluctuations, due the presence of a potential well deep inside particle overlapping. In the very early stages of the quenching dynamics, the system can be viewed as being comprised of (randomly oriented) oscillating dipoles, whose typical frequency is dictated by the thermal fluctuations around their equilibrium positions. As many-body correlations start to set-in, such dipoles start to merge into larger aggregates, the dynamics of which is controlled not only by the strength of the electrostatic interactions, but also by the degree of particle penetration (see ESI†). Indeed, the overall effect of the electrostatic interactions in this case is to achieve local charge neutrality. If the particle stiffness is sufficiently weak, oppositely charged particles will partially neutralize their individual charges upon mutual overlapping. As a consequence, we expect that soft particles will cluster into compact aggregates in an attempt to achieve local charge neutrality, whereas rigid particles will assemble into more open structures with typical local ordering. Apart from this simple picture, the interplay between soft repulsion and electrostatic interactions will also influence the way particle aggregates will be arranged in order to minimize their multi-pole charges, rendering the whole self-assembly process very complex.

We start by looking at the dynamics of cluster formation after the quenching process. To this end, we identify particle clusters by defining that a pair of particles whose distance at a given time is smaller than the cut-off distance $R_c = 1.25\sigma$ should belong to the same cluster. This cut-off distance is short enough to guarantee that all particles within the same cluster are strongly inter-connected. Fig. 4 shows the time evolution of the total number of clusters N_c for microgel charges Z = 300 (upper panels) and Z = 500 (lower panels). This quantity provides us with valuable information on the global self-assembly properties. Although the dynamics of cluster formation is quite different for different system parameters, we can see that in most cases the particles will all combine into one single cluster at sufficiently long simulation times. These single clusters can be structured as either one compact aggregate or be assembled into a percolating network which spans the whole simulation box – a clear signature of arrested gel-like formation. It is quite clear from Fig. 4 that the dynamics of cluster formation strongly depends on the

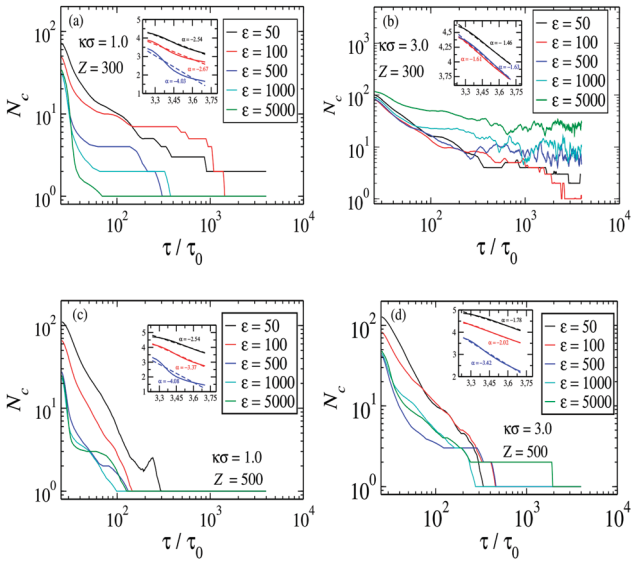

Fig. 4 Total number of clusters N_c as a function of simulation time step τ (in units of $\tau_0 = \sqrt{m\beta\sigma^2}$). The curves have been slightly smoothed by averaging this quantity over time intervals of $5\tau_0$. By definition, a pair of particles are considered to belong to the same cluster if their distance is shorter than the cut-off radius $R_c = 1.25\sigma$. Upper panels correspond to the microgel charge $Z = 300$, whereas in the lower panels the case $Z = 500$ is shown. The inverse Debye screening length is $\kappa\sigma = 1$ for the left panels, and $\kappa\sigma = 3$ for the right-hand panels.

strength of electrostatic forces. At sufficiently strong electrostatic couplings (namely high charges and/or long screening lengths κ^{-1}), the initial dipole pairs quickly merge together to form bigger structures characterized by complex internal charge distributions (see Fig. 4c). This process of dynamic cluster growth is slowed down as the electrostatic interactions get weaker. It is important to notice that the particle stiffness also plays a similar role in the dynamics of cluster formation. As the particles become softer and start to interpenetrate one another, the charge inhomogeneity results in multipole interactions with a reduced strength, in such a way that different clusters will take more time to stick together. In the case of smaller electrostatic coupling $Z = 300$ and $\kappa\sigma = 3$, the system is no longer able to organize into one single cluster, even at very long simulation times (Fig. 4b).§ In this case, the particles are assembled into amorphous, charge neutral individual clusters which interact very weakly. We notice that the particle softness plays a somewhat different role in this situation: the very weak electrostatic interactions make it more difficult for stiffer particles to stick together, rendering the clustering process rather unstable and resulting into a tendency to have the particles rather dispersed in the solution.

When particle stiffness becomes sufficiently weak, the early stages of aggregation kinetics can be fairly well described by a process similar to that of a Diffusion-Limited Aggregation (DLA) in binary systems: whenever two oppositely charged particles meet each other, they will most likely stick together, resulting in the merging of small clusters such as dimers and tetramers. This aggregation process leads a to well-known dynamic scaling regime in which the number of clusters decays as power-law as time evolves. The insets in Fig. 4 highlight this regime by showing the linear decay of $\ln(N_c)$ with $\ln(\tau/\tau_0)$ at the initial stages of cluster aggregation. The corresponding scaling exponents, extracted from a linear fitting in this regime, are also shown. This simple scaling decay start to break down at time scales where particles start to reorganize within the clusters in such a way as to minimize the interaction between the larger, charge neutral aggregates. It is important to emphasize that this regime can be only observed when particles are soft enough such that the event of encountering between oppositely charged particles leads to cluster aggregation.

Having analyzed the overall dynamics of cluster formation, we now turn the local dynamic properties within the clusters. One relevant quantity that characterizes the local environment surrounding each particle is provided by the average number of nearest neighbors that each particle possess, n_b. Here we employ the definition that two particles are considered as nearest neighbors if their center-to-center distance is smaller than the cut-off distance $R_{cn} = 1.1\sigma$. Besides, only particles with different charges can be considered as being closest neighbors. Notice that the cut-off distance of closest neighbors is smaller than that used to identify particles belonging to the same cluster. This stricter constraint should ensure that only particles that are electrostatically bound to each other will be considered as neighboring particles. The more compact the local cluster structure is, the larger the number of closest neighbors around particles in the cluster will be. In this case of compact, closed structures, it is important to bear in mind that this quantity can be quite susceptible to the cluster surface area, as particles belonging to the surface face an asymmetric environment, in opposition to those at the cluster core. Fig. 5 displays the average number of nearest neighbors as a function of simulation time for the system parameters under consideration. In the case of the smallest charge $Z = 300$ (upper panels) two different regimes can be clearly distinguished, depending on the screening length. At moderate inverse screening length $\kappa\sigma = 1$, the local structure as measured by the number of closest neighbors is very little sensitive to particle stiffness, especially at the limit of long simulation times. On average, each particle is surrounded by 4 to 5 oppositely charged neighbors in this regime. The local arrangement of these neighboring particles should however be sensitive to particle softness. While soft particles will strongly overlap their oppositely charged neighbors – given thus rise to amorphous local charge arrangements – stiff particles should on the other hand stick together at close to contact distance, leading to local charge ordering. Once again, the case of smallest charge and strong screening $\kappa\sigma = 3$ displays a somewhat different behavior, whereby the stiffer particles have on average a smaller number of neighbors (see Fig. 5b). This is because the strongly repulsive, short-ranged interactions prevent these particles from associating into large clusters due to the weaker electrostatic bounding energy at contact, resulting in smaller-sized clusters,

§ Although the system is naturally characterized by longer relaxation times in this case, it seems very unlike that any single cluster morphology will be stable due to the strong thermal susceptibility at such low electrostatic coupling.

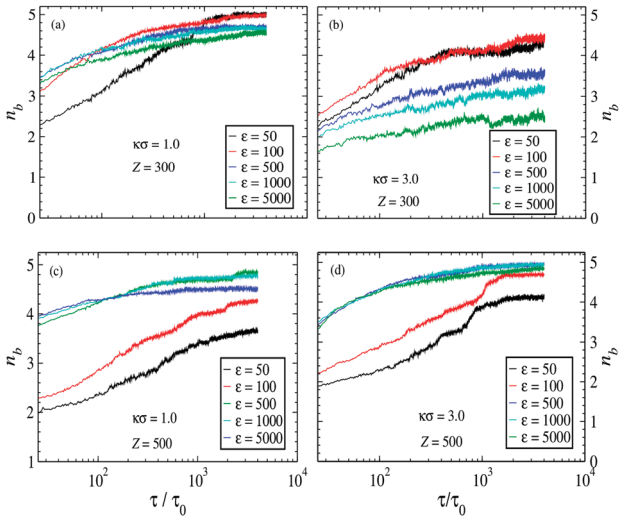

Fig. 5 Averaged number of closest neighbors around each microgel as a function of simulation time (in units of τ_0) for different strengths ε of the elastic repulsion. The corresponding system parameters are: Z = 300 and κ = 1.0 (a), Z = 300 and κ = 3.0 (b), Z = 500 and κ = 1.0 (c) and Z = 500 and κ = 3.0 (d).

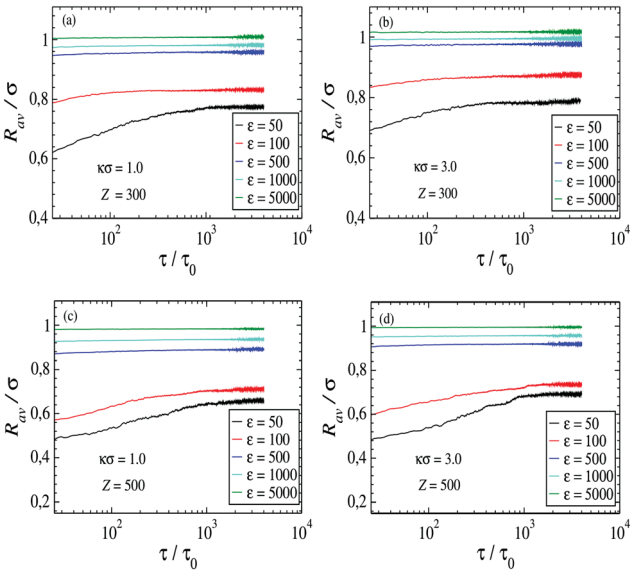

Fig. 6 Averaged center-to-center distance of closest neighbors, as defined by eqn (8), at different particle softness, charges and screening lengths.

as revealed by Fig. 4b. For the higher charge Z = 500 (lower panels) the stiff particles ($\varepsilon \geq 500$) display almost indistinguishable behaviors, regardless the screening length. Here however a different local arrangement of soft particles ($\varepsilon \leq 100$) can be distinguished. For weak screening, the average number of neighbors is rather small, suggesting the presence of open-like cluster structures (Fig. 5c). A similar behavior can be also seen in the case of stronger screening (Fig. 5d) up to a certain time ($\tau/\tau_0 \approx 2000$) where the number of neighbors undergoes a sudden increase. This steep increase in the number of nearest can be assigned to the folding of open structures (high surface areas) into a compact cluster (smaller surface area), leading to many local particle rearrangements.

Although the particle stiffness has little influence on the local number of oppositely charged neighbors at the close contact to a target particle, it does certainly affect the distances of closest approach distance between them. In order to quantitatively analyze this effect, we have measured the averaged distance R_{av} between closest neighbors at each time step. This quantity measures how close neighboring particles within a cluster are, and is defined as

$$\langle R_{\mathrm{av}}(\tau)\rangle = \frac{1}{2N_{\mathrm{p}}}\sum_{i=1}^{N}\sum_{j} r_{ij}(\tau), \qquad (8)$$

where r_{ij} is the distance between particles i and j at the simulation time τ, and N_{p} is the total number of neighboring pairs. The sum over j is performed on the set of closest neighbors to particle i, and the factor 1/2 is introduced to avoid double-counting of neighboring distances. Soft particles will be obviously able to penetrate each other more significantly than hard ones, leading to close-packed local arrangements and shorter inter-particle separations. This general trend is clearly confirmed in Fig. 6, in which time dependence of the averaged nearest-neighbor distances for different electrostatic couplings and particle stiffness is shown. Some quite general conclusions can be drawn regarding the effects of the considered system parameters on particle interpenetration. For dimensionless Hertzian strengths of order $\mathcal{O}(10^3)$, the short repulsion is strong enough to suppress any considerable degree of particle penetration, even at the highest electrostatic coupling considered. In this regime, the system behavior resembles that of a binary sticky hard-sphere fluid with equal (renormalized) particle diameters. Once two such oppositely charged particles become electrostatic bound to each other, they remain stuck together at well defined radial separations. Although these bounded particles are able to detach as cluster dynamics proceeds, the mean separation between closest neighbors will remain almost constant during time evolution (Fig. 6). Soft microgels, on the other hand, display a quite different dynamic behavior regarding they mean close-contact distances, with typical longer relaxation times. In the very early stages of quenching dynamics, the soft nanoparticles ($\varepsilon \leq 100$) overlap considerably (up to $R_{\mathrm{av}} \approx 0.5\sigma$ for highest electrostatic couplings), in a clear attempt to maximize local charge neutrality by forming pairs. This results in a system where 2-particles clusters interact with a much weaker effective dipole interaction that continues to drive the aggregation process, albeit slower, and where particles in the larger aggregates overlap with multiple neighbors of the opposite charge at the cost of an increased binding distance in order to prevent like-wise charge overlaps. This process continues until a steady state at long simulation times is reached, but even in such "stabilized" configurations, a strong degree of particle overlapping can be observed.

Another interesting observation that can be made from the dynamics of inter-particle distances is the fact that this quantity is almost insensitive to changes in the screening of electrostatic interactions, as revealed by a direct comparison between

left ($\kappa\sigma$ = 1) and right ($\kappa\sigma$ = 3) panels of Fig. 6. This result is quite consistent with the underlying physical picture of particle overlapping: as two or more microgels are brought together in close contact, their interactions will be almost unscreened as very few screening counterions are enclosed within such small center-to-center distances. The degree of electrostatic screening plays therefore a minor role in determining the close-contact distances, which are thus dictated by particle charge and stiffness. It is important however to emphasize that the screening length does play a very important role in the overall dynamics of cluster formation, as has been already shown in Fig. 4 and 5.

Although the number of closest neighbors and their relative radial distances provide important information on the local structures within the particle agglomerates, these quantities do not give us information regarding the correlations in the relative orientations of these neighborhoods – essential to investigate the local structural ordering. In order to access this information, we have measured an orientational order parameter $d_l(i,j)$ between neighbors i and j, which provides valuable information on how correlated the local relative orientations are. This order parameter is defined by the dot product $d_l(i,j) = \mathbf{q}_l(i)\cdot\mathbf{q}_l^*(j)$ of the vector order parameters $\mathbf{q}_l$ corresponding to closest neighbors i and j. The elements of these (complex valued) $2l + 1$-dimensional vector local order parameters are defined as

$$q_l^m(i) = \frac{1}{n_b(i)} \frac{\sum_j Y_l^m(\hat{\mathbf{r}}_{ij})}{\sqrt{\mathbf{q}_l(i)\cdot\mathbf{q}_l^*(i)}}, \qquad (9)$$

where $q_l^m(i)$ denotes the m-th element of $\mathbf{q}_l(i)$ corresponding to particle i ($-l \le m \le l$), Y_l^m are normalized spherical harmonics of rank l and $\hat{\mathbf{r}}_{ij}$ is the unit vector connecting the center of neighboring particles i and j. The summation on the right-hand-side of this expression is performed over the set of $n_b(i)$ closest neighbors of particle i. Notice that the local order parameters $\mathbf{q}_l(i)$ are normalized to unity according the definition (9). As a consequence, the local order parameter $d_l(i,j)$ (which is, by construction, a real quantity) can only assume values smaller than unity. This quantity clearly measures the degree of orientational correlation between neighborhoods of nearest neighbors.[80,81] Whenever two neighboring particles are embedded in an identical local environment (as in some typical crystalline structures), all their connecting vectors $\hat{\mathbf{r}}_{ij}$ will be the same, and the local order parameter $d_l(i,j)$ will be equal to unity. In cases where the local structures surrounding two closest particles are slightly different from one another, the corresponding local order parameter will deviate only slightly from unity. This quantity give us therefore information on the local orientation inter-connection between closest neighbors. Furthermore, the distribution of this quantity provides well defined signatures of many typical solid-like arrangements.[80,81]

Two neighboring particles i and j are considered to be connected, or bonded together, when the corresponding orientational order parameter $d_l(i,j)$ is larger than a given threshold value. The criteria for choosing this value depends on the typical local arrangements of solid-like structures, as well as on the rank l assigned to the vector order parameters $\mathbf{q}_l(i)$. Here we take l = 6, and consider two neighboring particles i and j as being connected if their mutual orientational local order parameter is larger than 0.7. The larger the number of such connected particles in the system, the stronger the local crystalline order will be. In particular, we can define a given particle as belonging to a solid-like environment if it is connected to a given number of its nearest neighbors. Again, the choice of this number is not unique, and depends on the topology of the typical crystalline structures at hand. We will adopt here the convention that a particle will be solid-like if it is connected to the majority of its neighbors (*i.e.*, at least half plus one of them) and if it has more than 4 nearest neighbors. Notice that this criteria allows particles located at the cluster boundaries to be consider as solid as well. Moreover, it avoids particles belonging to dipole pairs or chain-like formations to be considered as solid-like.

The dynamic evolution of the fraction of such solid-like particles after quench is displayed in Fig. 7. Since the orientational order parameter is quite sensitive to thermal fluctuations (as particles continuously change their local relative orientation due to their natural vibration modes) the fraction of solid-particles has been time-averaged over $150\tau_0$ time steps. Still, large fluctuations of this quantity can be observed, particularly at weak electrostatic couplings, whereby the relatively weaker electrostatic interactions at close contact makes the emergence of local orientational ordering rather unstable. This is to be contrasted with the radial inter-particle separation, which is much more stable against thermal fluctuations, and characterized by shorter equilibration times (Fig. 6). Furthermore, the orientational order parameter is expected to be strongly sensitive to the underlying cluster sizes, as the merging (or detachment) of big clusters should be accompanied by local particle rearrangements. An interesting case is the one corresponding to system parameters Z = 300 and $\kappa\sigma$ = 1 (Fig. 7a). For very loose nanoparticles (ε = 50), the system is unable to achieve any considerably degree of local ordering (black curve in Fig. 7a) until very long simulation times, when amorphous clusters start to merge into larger aggregates with a higher degree of local ordering. The situation changes drastically when the Hertzian strength is increased to ε = 100, whereby a large degree of particle ordering is achieved. Here, the fraction of solid particles undergoes an abrupt "jump" at intermediate time steps ($\tau \approx 10^3\tau_0$), displaying a high degree of local orientational order. This rapid increase in local ordering follows the quick merging of several small clusters into bigger ones (see Fig. 4), which decrease the overall surface area and force particles to locally re-orient themselves. By further increasing the particle stiffness, the resulting decrease in the electrostatic contact energy leads to structures which are (on average) locally less ordered. A similar trend is observed when the microgel charge is increased to Z = 500 (see Fig. 7c), the local order being reduced upon increasing of particle stiffness. In this case, however, the high electrostatic coupling makes particles to quickly merge together to form single aggregates, allowing them to organize into more

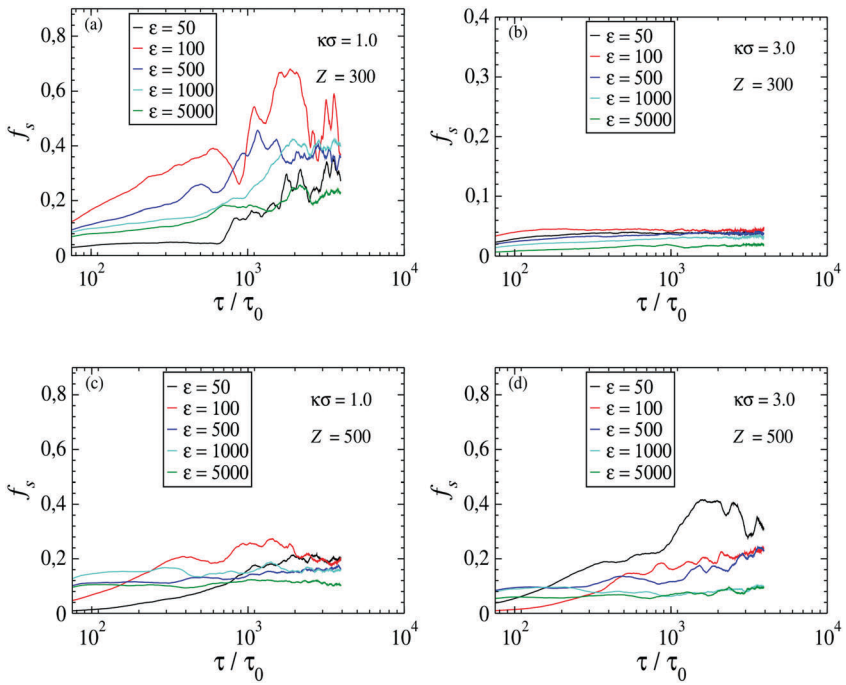

Fig. 7 Dynamic evolution of the fraction of particles belonging to a solid-like environment, f_s, for different system parameters.

stable local structures. The degree of local ordering is however smaller as compared to the situation of weakly charged particles, $Z = 300$. This result sounds somewhat counterintuitive: one expects that higher electrostatic couplings should lead to local ordered structures. This reduction of local crystallinity can be assigned to the observed tendency of these systems to self-assemble into open, percolated structures, for which the level of local ordering is smaller in comparison to compact aggregates. As the electrostatic interactions become more screened (right-hand panels), the degree of local ordering is decreased. This effect is much more pronounced in the case of weaker electrostatic coupling (Fig. 7b), for which local bounding is almost completely absent at all particle softness. The fact that local ordering tends to break down as interactions get more screened is in fact not so surprising. A deviation from this general trend is however observed in the case where $Z = 500$ and $\varepsilon = 50$ (see Fig. 7d). In this case, an increase in κ leads to more ordered local structures. This increase in local ordering can be assigned to the concomitant collapse of percolated chain-like structures into multi-layered open clusters, as revealed by a close look at the morphology of cluster formations in Fig. 3.

6 Static properties

Having analyzed the dynamic behavior of the symmetric binary system, we now turn to the investigation of its static properties, as obtained by time-averaging suitable quantities. In order to ensure that such averages are performed over equilibrium configurations alone, we have restricted the time-averages to simulation times larger than $1000\tau_0$. One relevant quantity that provides useful information on the overall particle structure is the well-known radial pair correlation function $g_{ij}(r)$ which measures the relative probability of finding a pair of particles of component i and j at a radial separation r with respect to that in an ideal gas.

The pair correlations functions for both symmetric (++) and asymmetric (+−) charged components are shown in Fig. 8 for cases of weak ($\varepsilon = 100$, upper row), moderate ($\varepsilon = 500$ middle row) and strong ($\varepsilon = 5000$ lower row) Hertzian strengths. In all cases, the electrostatic coupling decreases as we go from the left to the right panels. A close look at the behavior of these radial distributions as both stiffness and electrostatic strengths increase reveals some quite interesting, general trends. We first notice that the heights of first peaks of the pair correlations are generally very high for the considered system parameters, indicating that the system is in all cases far from equilibrium liquid-like phases. Secondly we note that, as the strength of Hertzian elastic repulsion increases (upper to lower panels), the height of the first peak of $g_{ij}(r)$ increases for oppositely charged particles (red curves), whereas it decreases in the case of equally charged particles (black lines). Concomitantly, the main peak of $g_{+-}(r)$ becomes increasingly sharp, while the peak of $g_{++}(r)$ (or equivalently $g_{--}(r)$) broadens up. Both effects are more pronounced in the case of higher electrostatic couplings. All these observations are a clear indication that the competition between attractive and repulsive interactions between oppositely/equally charged particles are enhanced as the particles become more loose. The physical interpretation of this general behavior is indeed quite straightforward: as soft particles are allowed to come closer to each other (notice also that the main peaks are shifted rightwards as ε increases), the distance between equally

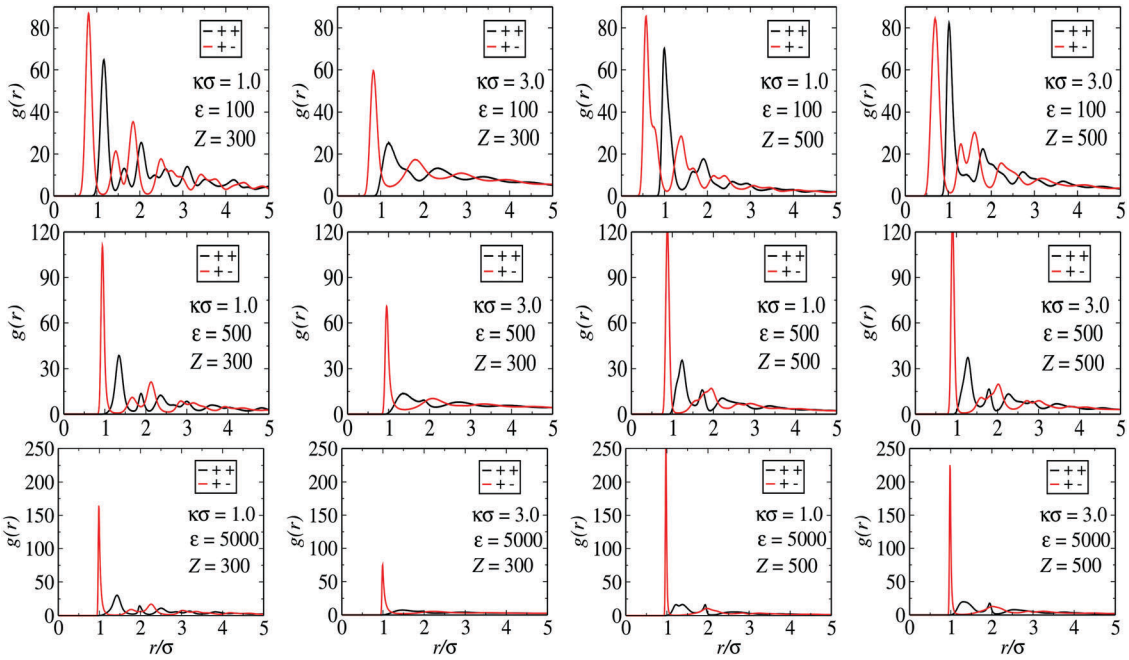

Fig. 8 Radial distribution functions corresponding to symmetric (black curves) and asymmetric (red curves) charged pairs, at different system parameters. The top row corresponds to Hertzian parameter $\varepsilon = 100$, while the middle row stands for $\varepsilon = 500$ and the bottom panels are results for $\varepsilon = 5000$. The electrostatic couplings are described by microgel charges $Z = 300$ (first and second columns) and $Z = 500$ (third and fourth columns) and inverse Debye screening lengths of $\kappa\sigma = 1$ (first and third columns) and $\kappa\sigma = 3$ (second and fourth columns).

charged neighboring particles will also be much shorter, rendering their mutual repulsion much stronger. As a consequence, the charge ordering is also long-ranged in the case of soft particles. As particle stiffness is enhanced, the attractive interactions strongly dominates over the repulsive ones, and the system structure is mostly dictated by the propensity of unlikely charged particles to come in close contact to each other. The fact that the mean separation between closest neighbors is broader for soft particles could have been already anticipated from Fig. 5, which shows that soft particles firstly overlap each other considerably before finding their static equilibrium positions.

Finally, it is to be noted that, in spite of the shallow potential well for larger ε displayed in Fig. 1, the pair correlation functions feature more pronounced and thinner main peaks in this regime. This is due to the fact that the potential minima for stiffer particles are thinner (more localized) with respect to the case of smaller ε, and the inter-particle distances less susceptible to thermal fluctuations.

The fact that the competing repulsive and attractive electrostatic interactions become both stronger and more long-ranged for soft particles (as can clearly be seen in the first row of Fig. 8) indicates that the degree of charge ordering will be smaller in this case. Indeed, if oppositely charged particles are allowed to considerably overlap each other, the degree of local charge inhomogeneity in the system will decrease. Again, this is a manifestation of the general attempt of any charged system to achieve local charge neutrality (despite the fact that the fulfillment of this condition is, strictly speaking, thermodynamically unstable). The degree of charge inhomogeneity is on the other hand a very important quantity, since it dictates the way the system will respond to an external stimuli that couples with the local charge (*e.g.*, an external electric field). In order to access this information, we have measured the static charge–charge structure factor $S_{cc}(\mathbf{k})$ of the binary system, which is defined as:

$$S_{cc}(\mathbf{k}) = \sum_{ij} Z_i S_{ij}(\mathbf{k}) Z_j, \tag{10}$$

where Z_i is the total charge of component i, and $S_{ij}(\mathbf{k})$ represents the usual structure factor of components i and j. It is defined as

$$S_{ij}(\mathbf{k}) = \delta_{ij} + \sqrt{\rho_i \rho_j}\hat{h}_{ij}(\mathbf{k}), \tag{11}$$

the functions $\hat{h}_{ij}(\mathbf{k})$ being the Fourier transform of the total pair correlation functions $h_{ij}(r) = g_{ij}(r) - 1$. The structure factors of nanoparticles are readily accessible through light scattering measurements, and provide therefore a valuable link between theory and experiments. The charge–charge structure factors measures the degree of local charge rearrangement in response to electric fields characterized by spatial correlations of typical wavelengths $\lambda = 2\pi/k$. The larger the degree of structural charge inhomogeneity, the more susceptible the charges will be in responding to such fields. The charge–charge structure factors provide thus valuable information on the magnitude of charge ordering in a charged system. For the present case of a fully symmetric microgel system of charge Z interacting through a radially symmetric pair interaction, the charge–charge structure factors in eqn (10) read as:

$$S_{cc}(k) = Z^2[S_{++}(k) + S_{--}(k) - 2S_{+-}(k)]. \tag{12}$$

We have calculated these quantities by Fourier transforming the total distribution functions obtained from MD simulations.

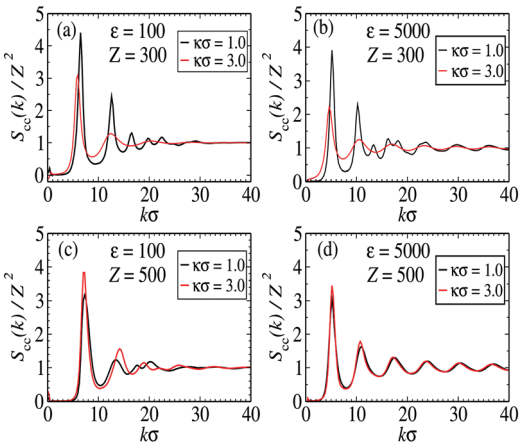

Fig. 9 Normalized charge–charge structure factors, S_{cc}/Z^2 as a function of inverse wavelength k for different system parameters. Upper panels correspond to particle charge Z = 300, whereas lower panels stand for Z = 500.

The results are shown in Fig. 9 for different ionic strengths and particle softness. Notice that the structure factors have been normalized by the squared particle charges in order to collapse all curves in a similar scale. This is justifiable since we are concerned with the signatures of charge ordering, rather than the absolute magnitude of these quantities. While the first peaks of the charge structure factors corresponds to long-ranged charge ordering, the emergence of secondary peaks at smaller wavelengths signals on the other hand the onset of local charge ordering. This trend can be clearly observed as the particle stiffness is increased (from left to right panels) in both cases of moderate (top panels) and large (bottom panels) particle charges. Indeed, a strong dependence of charge ordering on the degree of particle stiffness is found. Such dependence is stronger in the case of large electrostatic couplings, where the system achieves a large degree of charge ordering as the Hertzian strength grows larger (see Fig. 9d). Interestingly enough, the charge ordering displays quite opposite behavior in comparison to the local particle ordering: whereas the latter decreases with particle stiffness (see Fig. 7), the former becomes more pronounced at larger soft repulsions. The physical mechanisms behind such dependence on the particle stiffness are rather clear: as particles become more rigid, the spatial charge inhomogeneities get stronger – since oppositely charged particles will no longer be able to overlap each other and thereby neutralize their local charges. If particles are on other hand allowed to interpenetrate, they will become strongly bound to one another, leading to an increase in local particle ordering. Once again we notice that the screening of electrostatic interactions have a minor effect in the case of large charges (Z = 500), whereas for moderate charges (Z = 300) some qualitative differences in $S_{cc}(k)$ can be clearly distinguished.

A deeper understanding on the local particle arrangements can still be achieved by analyzing the averaged distribution of closest neighbors around a given particle. In Fig. 6 we have shown the dynamic evolution of the averaged number of nearest neighbors for different particle stiffness and electrostatic couplings. This quantity however provides us only with an overall picture of how local particle arrangements should (on average) look like. If for instance the system comprises of percolating clusters bearing dissimilar local particle arrangements, the averaged number of closest neighbors will not be a suitable quantity to describe the whole scenario of local particle arrangements. A more detailed analysis on the local morphology can thus be performed by looking at the time-averaged distribution of closest neighbors. To this end, we have measured the number of particles $n(i,\tau)$ which have exactly i closest neighbors at each time step τ. From this quantity we can define the time-averaged fraction of particles possessing i nearest neighbors as:

$$f(i) = \frac{1}{T-\tau_c}\int_{\tau_c}^{T}\frac{n(i,\tau)}{N}\mathrm{d}\tau, \qquad (13)$$

where $\tau_c = 10^3\tau_0$ is a cut-off simulation time, chosen such as to avoid average over out-of-equilibrium configurations, and T is the total simulation time. Fig. 10 shows the probability distribution of the number of closest neighbors for different particle stiffness and electrostatic couplings. Some interesting features can be highlighted from these probability distributions. First we notice that in most cases the distributions are rather broad, which is consistent with the physical picture of percolating clusters characterized by different local morphologies. Secondly, it is important to note that in the case of small charge (Z = 300, upper panels) the distribution of the number of neighboring particles is slightly shifted to the left as the particle stiffness increases. This results confirms what has been already indicated from an analysis of Fig. 5: soft particles tend to aggregate into very compact clusters with small surface area in this case – increasing the concentration of neighboring particles at the vicinity of a given microgel. The distribution is on the other hand shifted to the right with increasing ε in the case of larger microgel charge (Z = 500, lower panels). Again, this result is in accordance with

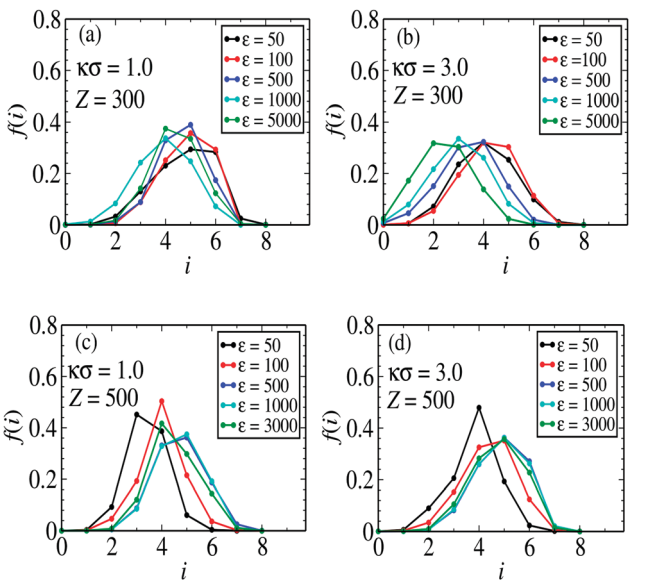

Fig. 10 Time-averaged probability distribution of the number of neighboring particles for different system parameters.

the conclusions outlined from Fig. 5: soft particles in this case assembly into open, inter-connected networks characterized by a low density of neighboring particles. Notice also that the distributions get sharper in the case of soft particles, indicating that the local arrangements are more stable over the whole system. These local structures seem to be quite sensitive to the range of electrostatic interactions: increasing of the inverse Debye screening length of soft particles leads to an overall increase of closest neighbors (see red curves in Fig. 10a and b). This suggests that the observed ''worm-like'' inter-connected structures are stabilized by a fine competition between attractive and repulsive interactions between closest similarly/dissimilarly charged particles along these networks – which break down as the repulsive interactions become screened. As a final remark, we point out that the fraction of isolated dipoles is relatively high in the case of the lowest electrostatic coupling (Fig. 10b), and is an increasing function of the particle stiffness. In the case of the strongest Hertzian repulsion (green curve) about 20% of the particles are found to have assembled into isolated dipolar pairs.

7 Conclusions

We have investigated the aggregation properties of a fully symmetric, binary system composed of oppositely charged microgels. A rich variety of self-assembly structures was found, and the dependence of their morphological properties on the different system parameters has been discussed at length. Particular attention has been given to the role played by the steric Hertzian repulsion on particle self-assembly. The interplay between such soft repulsive and electrostatic interactions is shown to be a key point in determining many aspects of particle aggregation. In contrast to purely hard-core interactions, the short-ranged elastic repulsion let particles to come in close contact to each other – way beyond overlapping – allowing for the formation of locally dense, compact aggregates which can not be formed in hard systems. This possibility of particle interpenetration is shown to enhance the competition between electrostatic attractive and repulsive interactions, as dissimilarly charged particles can come close to short distances. Besides, it also has a major influence on the degree of charge inhomogeneity along the entire system. As oppositely charged particles start to strongly penetrate one another, they partially neutralize their mutual charge in the overlapping region. This tendency of achieving local charge neutrality diminishes the charge inhomogeneity throughout the system, and leads to a decrease of charge ordering in comparison to the hard-sphere case.

The observed dependence of particle aggregation on the strength of soft repulsion has many practical implications, since the degree of particle stiffness can be experimentally tuned during the synthesis process of microgels. Loosely cross-linked microgels are softer in nature, whereas microgels synthesized with a high concentrations of cross-linkings will display a larger elastic repulsion upon contact. It might be argued on the other hand that the Hertzian repulsion is a rather heuristic approach to describe the elastic interactions, particularly when the degree of overlapping is high. Indeed, one expects that strongly compressed microgels will hardly retain they spherical shape. Such deviations from ideal sphericity may play an important role in particle aggregation, specially in the case of highly compact aggregates. Besides, microgel particles can undergo size fluctuations by changing their internal polymeric conformation upon strong mutual compressions.[82] None of these effects are taken into account at the Hertzian level of approximation. A proper description of the interplay between shape and volume changes is however a rather challenging task,[83] and would certainly compromise the clarity and physical transparency underlying the Hertzian approach. In spite of these deficiencies, the proposed model is able to provide valuable insights in the overall effects of particle stiffness on the self-assembly behavior.

Unfortunately, to date and the best of our knowledge few experimental results exist capable of testing the validity of the assumptions underlying the present model system. We hope that the interesting self-assembly behavior shown by our simulations will motivate further experimental studies on these type of similar systems. Although the accuracy of the proposed model can be questionable in describing microgels with a high degree of cross-linking, we believe that the overall qualitative effects of triggering the competition between soft elastic and electrostatic interactions on particle self-assembly should be accurate enough in a wide range of experimentally-achievable system parameters and provide an indication of the correct behavior in the more extreme cases.

Another important point to be addressed regarding the model system is the underlying approximation of a uniform internal charge distribution assigned to the microgels. Although this assumption of homogeneous charge is a reasonably approximation for purely repulsive systems – which tend not to come to close contact at all – it might be an oversimplification in the case of attractive interactions. In fact, as microgels overlap each other, one expect from energetic considerations that a fraction of their polymer backbones will be expelled out from the overlapping region. As a consequence, the internal charge distribution should become patchy-like, deviating considerably from uniformity. Whether these effects would significantly change the aggregation properties is a difficult question. To overcome this deficiency, a model system can be devised in which the microgels are allowed to change their internal charge conformation in response to an external field that mimic particle interactions – in addition to an elastic penalty. This is, however, beyond the scope of the present work and left for future research.

As a final remark, we observe that the model system can be used to investigate asymmetric binary systems as well. By changing the asymmetry of system parameters such as relative particle concentrations, size and charge, a richer variety of aggregation scenarios should be induced. Furthermore, the relative strength of the Hertzian parameter can be made asymmetric as well. Mixing particles with different softness can be a promising strategy to take advantage of the observed aggregation dependence on particle stiffness to trigger different self-assembly compositions.

Conflicts of interest

There are no conflicts to declare.

Acknowledgements

This work is dedicated to the memory of Per Linse, a great scientist and unforgettable colleague, whose outstanding contributions in soft matter, and in particular for charged systems, have brought about tremendous advances in the field. This work has been supported in part by the European Training Network COLLDENSE (H2020-MCSA-ITN-2014, Grant No. 642774). Calculation time at the Vienna Scientific Cluster is gratefully acknowledged.

References

1 G. van Anders, D. Klotsa, A. S. Karas, P. M. Dodd and S. C. Glotzer, *ACS Nano*, 2015, **9**, 9542–9553.
2 E. Duguet, A. Desert, A. Perro and S. Ravaine, *Chem. Soc. Rev.*, 2011, **40**, 941–960.
3 J. P. K. Doye, A. A. Louis, I.-C. Lin, L. R. Allen, E. G. Noya, A. W. Wilber, H. C. Kok and R. Lyus, *Phys. Chem. Chem. Phys.*, 2007, **9**, 2197–2205.
4 C. N. Likos, *Soft Matter*, 2006, **2**, 478–498.
5 K. Thorkelsson, P. Bai and T. Xu, *Nano Today*, 2015, **10**, 48–66.
6 M. A. Boles, M. Engel and D. V. Talapin, *Chem. Rev.*, 2016, **116**, 11220–11289.
7 D. Fusco and P. Charbonneau, *Colloids Surf., B*, 2016, **137**, 22–31.
8 A. Stradner, H. Sedgwick, F. Cardinaux, W. C. K. Poon, S. U. Egelhaaf and P. Schurtenberger, *Nature*, 2004, **432**, 492–495.
9 W. C. K. Poon, *J. Phys.: Condens. Matter*, 2002, **14**, R859.
10 A. Yethiraj and A. van Blaaderen, *Nature*, 2003, **421**, 513–517.
11 S. C. Glotzer, M. J. Solomon and N. A. Kotov, *AIChE J.*, 2004, **50**, 2978–2985.
12 L. K. Mansson, J. N. Immink, A. M. Mihut, P. Schurtenberger and J. J. Crassous, *Faraday Discuss.*, 2015, **181**, 49–69.
13 J. J. Crassous, M. Ballauff, M. Drechsler, J. Schmidt and Y. Talmon, *Langmuir*, 2006, **22**, 2403–2406.
14 G. M. Conley, A. Philippe, S. Nöjd, P. Schurtenberger and F. Scheffold, *Sci. Adv.*, 2017, **3**, e1700969.
15 C. R. Murthy, B. Gao, A. R. Tao and G. Arya, *Nanoscale*, 2015, **7**, 9793–9805.
16 C. N. Likos, *Phys. Rep.*, 2001, **348**, 267–439.
17 F. A. Escobedo, *Soft Matter*, 2014, **10**, 8388–8400.
18 J. M. Lopez-Lopez, A. Schmitt, A. Moncho-Jorda and R. R. Hidalgo-Alvarez, *Soft Matter*, 2006, **2**, 1025–1042.
19 C. Valeriani, E. Sanz, P. N. Pusey, W. C. K. Poon, M. E. Cates and E. Zaccarelli, *Soft Matter*, 2012, **8**, 4960–4970.
20 D. F. Schwanzer and G. Kahl, *J. Phys.: Condens. Matter*, 2010, **22**, 415103.
21 N. E. Valadez-Perez, R. Castaneda-Priego and Y. Liu, *RSC Adv.*, 2013, **3**, 25110–25119.
22 M. B. Sweatman, R. Fartaria and L. Lue, *J. Chem. Phys.*, 2014, **140**, 124508.
23 N. I. Lebovka, in *Aggregation of Charged Colloidal Particles*, ed. M. Müller, Springer Berlin Heidelberg, Berlin, Heidelberg, 2014, pp. 57–96.
24 D. Pini and A. Parola, *Soft Matter*, 2017, **13**, 9259–9272.
25 M. A. Miller and D. Frenkel, *J. Phys.: Condens. Matter*, 2004, **16**, S4901.
26 A. Jamnik, *Chem. Phys. Lett.*, 2006, **423**, 23–29.
27 J. Largo, M. A. Miller and F. Sciortino, *J. Chem. Phys.*, 2008, **128**, 134513.
28 L. Belloni, *J. Phys.: Condens. Matter*, 2000, **12**, R549.
29 A. R. Denton, in *Effective Interactions in Soft Materials*, ed. A. V. Zvelindovsky, Springer, Netherlands, Dordrecht, 2007, pp. 395–433.
30 P. Schurtenberger, Proceedings of the International School of Physics ''Enrico Fermi'': Soft Matter Self-Assembly, 2016, pp. 81–136.
31 E. Brini, E. A. Algaer, P. Ganguly, C. Li, F. Rodriguez-Ropero and N. F. A. van der Vegt, *Soft Matter*, 2013, **9**, 2108–2119.
32 N. J. H. Dunn and W. G. Noid, *J. Chem. Phys.*, 2015, **143**, 243148.
33 S. Torquato, *Soft Matter*, 2009, **5**, 1157–1173.
34 A. F. Hannon, Y. Ding, W. Bai, C. A. Ross and A. Alexander-Katz, *Nano Lett.*, 2014, **14**, 318–325.
35 R. B. Jadrich, J. A. Bollinger, B. A. Lindquist and T. M. Truskett, *Soft Matter*, 2015, **11**, 9342–9354.
36 R. B. Jadrich, B. A. Lindquist and T. M. Truskett, *J. Chem. Phys.*, 2017, **146**, 184103.
37 E. Zaccarelli, *J. Phys.: Condens. Matter*, 2007, **19**, 323101.
38 P. J. Lu, E. Zaccarelli, F. Ciulla, A. B. Schofield, F. Sciortino and D. A. Weitz, *Phys. Rev. Lett.*, 2007, **99**, 118301.
39 P. J. Lu, E. Zaccarelli, F. Ciulla, A. B. Schofield, F. Sciortino and D. A. Weitz, *Nature*, 2008, **453**, 499–503.
40 E. Dickinson, *Adv. Colloid Interface Sci.*, 2013, **199-200**, 114–127.
41 S. Sennato, D. Truzzolillo, F. Bordi, F. Sciortino and C. Cametti, *Colloids Surf., A*, 2009, **343**, 34–42.
42 E. R. Russell, J. Sprakel, T. E. Kodger and D. A. Weitz, *Soft Matter*, 2012, **8**, 8697–8703.
43 R. Zhang, P. K. Jha and M. O. de la Cruz, *Soft Matter*, 2013, **9**, 5042–5051.
44 K. J. M. Bishop, N. R. Chevalier and B. A. Grzybowski, *J. Phys. Chem. Lett.*, 2013, **4**, 1507–1511.
45 A. F. Demirörs, J. C. P. Stiefelhagen, T. Vissers, F. Smallenburg, M. Dijkstra, A. Imhof and A. van Blaaderen, *Phys. Rev. X*, 2015, **5**, 021012.
46 T. Cao, T. Sugimoto, I. Szilagyi, G. Trefalt and M. Borkovec, *Phys. Chem. Chem. Phys.*, 2017, **19**, 15160–15171.
47 Y. Levin, *Rep. Prog. Phys.*, 2002, **65**, 1577.
48 R. Pelton and T. Hoare, *Microgels and Their Synthesis: An Introduction*, Wiley-VCH Verlag GmbH & Co. KGaA, 2011, pp. 1–32.
49 A. Fernández-Barbero, I. J. Suárez, B. Sierra-Martín, A. Fernández-Nieves, F. J. de las Nieves, M. Marquez, J. Rubio-Retama and E. López-Cabarcos, *Adv. Colloid Interface Sci.*, 2009, **147–148**, 88–108.

50 F. A. Plamper and W. Richtering, *Acc. Chem. Res.*, 2017, **50**, 131–140.
51 B. P. Tripathi, N. C. Dubey and M. Stamm, *ACS Appl. Mater. Interfaces*, 2014, **6**, 17702–17712.
52 T. Kureha and D. Suzuki, *Langmuir*, 2018, **34**, 837–846.
53 J. Zhang, S. Xu and E. Kumacheva, *J. Am. Chem. Soc.*, 2004, **126**, 7908–7914.
54 Y. Lu, S. Proch, M. Schrinner, M. Drechsler, R. Kempe and M. Ballauff, *J. Mater. Chem.*, 2009, **19**, 3955–3961.
55 C. N. Likos, *Structure and Thermodynamics of Ionic Microgels*, Wiley-VCH Verlag GmbH & Co. KGaA, 2011, pp. 163–193.
56 Y. Levin, A. Diehl, A. Fernández-Nieves and A. Fernández-Barbero, *Phys. Rev. E: Stat., Nonlinear, Soft Matter Phys.*, 2002, **65**, 036143.
57 A. A. Polotsky, F. A. Plamper and O. V. Borisov, *Macromolecules*, 2013, **46**, 8702–8709.
58 A. Ghavami and R. G. Winkler, *ACS Macro Lett.*, 2017, **6**, 721–725.
59 M. Quesada-Pérez, J. Ramos, J. Forcada and A. Martín-Molina, *J. Chem. Phys.*, 2012, **136**, 244903.
60 T. Colla, C. N. Likos and Y. Levin, *J. Chem. Phys.*, 2014, **141**, 234902.
61 A. R. Denton and Q. Tang, *J. Chem. Phys.*, 2016, **145**, 164901.
62 L. G. Rizzi and Y. Levin, *J. Chem. Phys.*, 2016, **144**, 114903.
63 L. Rovigatti, N. Gnan and E. Zaccarelli, *J. Phys.: Condens. Matter*, 2017, **30**, 044001.
64 J. K. Oh, R. Drumright, D. J. Siegwart and K. Matyjaszewski, *Prog. Polym. Sci.*, 2008, **33**, 448–477.
65 M. Malmsten, *Microgels in Drug Delivery*, Wiley-VCH Verlag GmbH & Co. KGaA, 2011, pp. 375–405.
66 P. S. Mohanty, S. Nöjd, K. van Gruijthuijsen, J. J. Crassous, M. Obiols-Rabasa, R. Schweins, A. Stradner and P. Schurtenberger, *Sci. Rep.*, 2017, **7**, 1487.
67 P. S. Mohanty, A. Yethiraj and P. Schurtenberger, *Soft Matter*, 2012, **8**, 10819–10822.
68 S. Nöjd, P. S. Mohanty, P. Bagheri, A. Yethiraj and P. Schurtenberger, *Soft Matter*, 2013, **9**, 9199–9207.
69 P. S. Mohanty, P. Bagheri, S. Nöjd, A. Yethiraj and P. Schurtenberger, *Phys. Rev. X*, 2015, **5**, 011030.
70 A. Fernández-Nieves, J. S. van Duijneveldt, A. Fernández-Barbero, B. Vincent and F. J. de las Nieves, *Phys. Rev. E: Stat., Nonlinear, Soft Matter Phys.*, 2001, **64**, 051603.
71 T. Nicolai, *Colloids Surf., B*, 2016, **137**, 32–38.
72 D. Go, T. E. Kodger, J. Sprakel and A. J. C. Kuehne, *Soft Matter*, 2014, **10**, 8060–8065.
73 D. Suzuki and K. Horigome, *J. Phys. Chem. B*, 2013, **117**, 9073–9082.
74 N. N. Oskolkov and I. I. Potemkin, *Macromolecules*, 2007, **40**, 8423–8429.
75 M. Bier, R. Roij and M. Dijkstra, *J. Chem. Phys.*, 2010, **133**, 124501.
76 T. Colla and C. N. Likos, *Mol. Phys.*, 2015, **113**, 2496–2510.
77 J. Riest, P. Mohanty, P. Schurtenberger and C. N. Likos, *Z. Phys. Chem.*, 2012, **226**, 711–735.
78 A. R. Denton, *Phys. Rev. E: Stat., Nonlinear, Soft Matter Phys.*, 2003, **67**, 011804.
79 C. Hanel, C. N. Likos and R. Blaak, *Materials*, 2014, **7**, 7689–7705.
80 P.-R. ten Wolde, M. J. Ruiz-Montero and D. Frenkel, *Faraday Discuss.*, 1996, **104**, 93–110.
81 S. Auer and D. Frenkel, *J. Chem. Phys.*, 2004, **120**, 3015–3029.
82 M. Urich and A. R. Denton, *Soft Matter*, 2016, **12**, 9086–9094.
83 I. B. de Aguiar, T. van de Laar, M. Meireles, A. Bouchoux, J. Sprakel and K. Schroën, *Sci. Rep.*, 2017, **7**, 10223.

